Interface thermal conductivities induced by van der Waals interactions

ARTICLE TYPE

Cite this: DOI: 00.0000/xxxxxxxxxx

Interface thermal conductivities induced by van der Waals interactions†

H. M. Dong,‡[a] H. P. Liang,[b‡] Z. H. Tao,[c] Y. F. Duan,*[a] M.V. Milošević,[c,d*] and K. Chang[e*]

Received Date
Accepted Date

DOI: 00.0000/xxxxxxxxxx

The interface heat transfer of two layers induced by van der Waals (vdW) contacts is theoretically investigated, based on first-principles calculations at low temperatures. The results suggest that out-of-plane acoustic phonons with low frequencies dominate the interface thermal transport due to the vdW interaction. The interface thermal conductivity is proportional to the cubic of temperature at very low temperatures, but becomes linearly proportional to temperature as temperature increases. We show that manipulating the strain alters vdW coupling, leading to increased interfacial thermal conductivity at the interface. Our findings provide valuable insights into the interface heat transport in vdW heterostructures and support further design and optimization of electronic and optoelectronic nanodevices based on vdW contacts.

1 Introduction

As electronic devices shrink in size and become more powerful, management of heat dissipation has become increasingly crucial to ensure reliable performance. One major challenge in thermal management arises from high-density interfaces inside and outside micro-nano devices, where Kapitza thermal resistance can hinder heat transfer between layers [1,2]. Of particular interest are microscopic mechanisms for interfacial thermal transfer through van der Waals (vdW) contacts fabricated from novel low-dimensional materials. Experimental techniques such as scanning tunneling microscopy, suspension micro-thermal bridge, and micro-Raman spectroscopy have proven useful in accurately measuring interfacial heat transport in vdW interfaces [2]. The use of two-dimensional (2D) materials presents exciting possibilities for the creation of innovative nanodevices [3]. However, the corresponding theoretical investigations are still lagging.

An accurate understanding of interfacial heat transfer via vdW interaction is vital for the thermal management in these nano-heterostructures and for improving practical device applications. The interfaces by the vdW interactions differ significantly from conventional interfaces, such as wedded interfaces, since the interface is the device. 2D materials have unique out-of-plane acoustic (*ZA*) phonon modes with quadratic dispersion, providing a new channel for interfacial thermal transfer [4]. Very recently, it has been proposed that there is an additional way of vacuum heat transport, resulting from quantum fluctuations that also generate the forces behind vdW interactions [5]. Interestingly, scientists have discovered that weak vdW coupling can result in significant interface thermal conductivity [6]. Utilizing vdW interface switching enables engineers to improve and control interface thermal conductivities [7]. Strain engineering can also enhance the interface thermal conductance by a considerable amount [8]. The interface thermal conductance is proportional to the square of the adhesion energy of the vdW Si/Pt interface [9]. These investigations show that vdW force connections facilitate easier control of interface thermal conductivity.

The heat transfer via vdW interactions, with a particular focus on graphene-based ones, has captured significant interest in recent years. However, investigations regarding interface heat transfer between different layers, along with corresponding theoretical analyses, have remained quite limited to date. In addition, the inconsistent results of various experimental and simulation methods have been observed [10]. There is a consistent flow of significant new findings. Researchers have recently observed thermally induced rotation of graphene on hexagonal boron nitride (hBN) [11], within a vdW heterostructure. The interface thermal conductivity of graphene/hBN heterostructures is remarkably changed by the interlayer rotation angle. The spectral phonon transmission is mainly contributed by low-frequency phonons below 10 THz [12]. The detailed physical mechanisms behind this finding still need to be further explored. By leveraging vdW interfaces, enhanced and switchable nanoscale thermal conduction is achievable by utilizing bundles of boron nanoribbons [13]. The importance of investigating the interfacial thermal conductivity in vdW heterostructures using precise calculations of vdW cou-

* Corresponding authors
[a] *School of Materials Science and Physics, China University of Mining and Technology, Xuzhou 221116, China, Email: yifeng@cumt.edu.cn*
[b] *Beijing Computational Science Research Center, Beijing, 100193, China*
[c] *Department of Physics and NANOlab Center of Excellence, University of Antwerp, Groenenborgerlaan 171, 2020 Antwerp, Belgium*
[d] *Instituto de Física, Universidade Federal de Mato Grosso, Cuiabá, Mato Grosso 78060-900, Brazil; Email: milorad.milosevic@uantwerpen.be*
[e] *School of Physics, Zhejiang University, Hangzhou 310027, P. R. China, Email: kchang@zju.edu.cn*

† Electronic Supplementary Information (ESI) available: the phonon transmission coefficient, the net heat flux density, and the DFT calculated data for the applied stress (strain). See DOI: 10.1039/xxxxxx

‡ H. M. Dong and H. P. Liang contribute equally to this work.

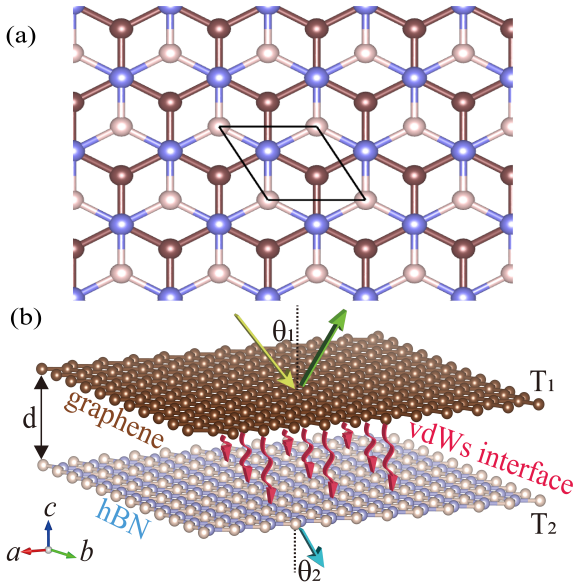

Fig. 1 (a) Top view of the AB-stacked graphene/hBN heterostructure. Brown, purple, and grey atoms represent C, B and N atoms, respectively. (b) Schematic depiction of thermal transfer in a graphene/hBN vdW heterostructure. $d = 3.3313$ Å is the optimized equilibrium interlayer distance along the z direction (c axis).

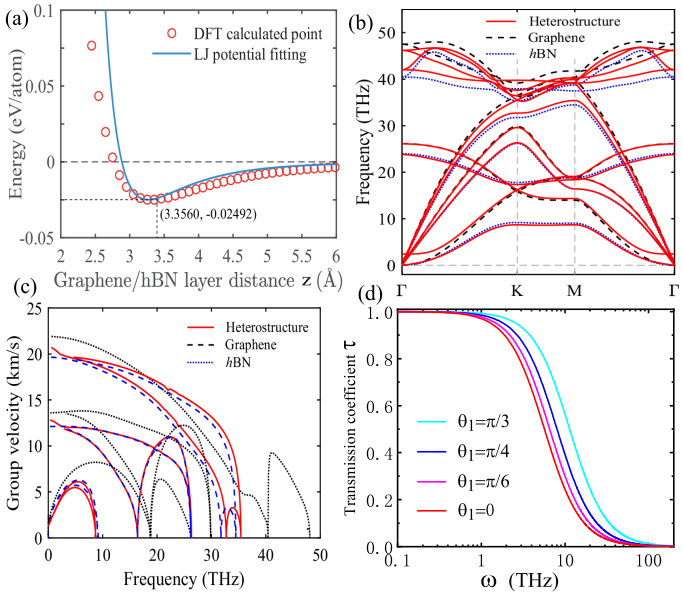

Fig. 2 (a) The vdW potential energy E in a graphene/hBN heterostructure, obtained by DFT calculations and LJ potential fitting with $\sigma = 2.99$ Å and $\varepsilon = 0.0249$ eV. The calculated phonon energy spectra (b) and the acoustic phonon group velocities (c) in graphene, hBN layer, and their heterostructure. (d) The transmission coefficient τ of the out-of-plane acoustic phonons as a function of the frequency ω for different angles θ_1 (cf. Fig. 1(b)).

pling cannot be emphasized enough. This is crucial for gaining a better understanding of heat transfer in fundamental nanoscale structures and has significant implications for developing and implementing nanodevices.

2 Theoretical model and results

To that goal, we first carried out first-principles calculations using density functional theory (DFT) in the Vienna ab initio simulation package (VASP)[14,15] with projector augmented-wave pseudopotentials[16,17]. The total energy is determined by using the PBE approximation and the plane-wave energy cutoff set at 550 eV[18]. The Brillouin zone is sampled using the Monkhorst-Pack scheme, and a Γ-centered k-point mesh of 12×12×1 ensures full relaxation of structures. We accounted for vdW interactions using the DFT-D3 method with the Becke-Johnson damping function[19,20]. A vacuum layer of 20 Å is specified. After relaxation, the graphene/hBN heterostructure exhibits an equilibrium lattice constant of 2.4857 Å, an interlayer distance of $d = 3.3313$ Å, and a total energy of $E = -9.1170$ eV/atom, as shown in Fig. 1.

To determine the total energy of each optimized structure, the distance between surfaces is adjusted and calculated at 0.1 Å increments from 1 Å to 11 Å, using a 6×6×1 k-point mesh. The energy data is changed based on the zero point of the potential energy at a distance of 11 Å, allowing for the acquisition of energy variation data for the graphene and hBN layers at different distances in Fig. 1(a) shown. After thorough trials of numerical approaches like optB86b-vdW, optB88-vdW, vdW-DF and DFT-D3, we have perceived a significant ascend in precision when using DFT-D3 in VASP to perform calculations of weak interactions. The DFT-D3 approach allows for atom pair energy contributions and tripartite adjustments, effectively improving accuracy without a cumbersome upsurge in computational effort.[19,20] Therefore, this method can be used as a general approach to studying interlayer interactions in vdW heterostructures. The interaction between pairs of atoms is described using the Lennard-Jones (LJ) potential[21], which is commonly used for the vdW interaction as

$$\phi(z) = -4\varepsilon\left[\left(\frac{\sigma}{z}\right)^6 - \left(\frac{\sigma}{z}\right)^{12}\right], \tag{1}$$

with ε the depth of the potential well and σ the length scale parameter. The two parameters ε and σ can be fitted with the DFT calculated data as shown in Fig. 2(a). We find the optimized equilibrium nearest distance $d = 3.3316$ Å between the layers 1 and 2, $\varepsilon = 0.0249$ eV/atom, and $\sigma = 2.99$ Å.

The application of the vdW interface with the harmonic approximation is utilized for modeling the interfacial contact in vdW heterostructures[9,13]. The vdW spring constant K between the two layers is represented by

$$K = \left(\frac{\partial^2\phi}{\partial z^2}\right)_{z=z_0} = \frac{72\varepsilon}{2^{1/3}\sigma^2}, \tag{2}$$

with $z_0 = 2^{1/6}\sigma$ being the equilibrium nearest neighbor atomic separation. In particular, by fitting between first-principles calculations and the LJ potential, $K = 0.159$ eV/Å^2 is calculated for graphene/hBN heterostructures.

The phonon dispersions and the second-order interatomic force constants (IFCs) were calculated using the Phonopy package[22]. The second-order IFCs are evaluated using the $8 \times 8 \times 1$ supercells with a Γ-centered k-point mesh of $1 \times 1 \times 1$. The phonon group velocities were calculated by Phonopy as $v_g(q_\nu) = \nabla_q \omega(q_\nu)$, where q_ν is the wave factor with the band index ν. The maximum

phonon group velocities were selected the data near the center of Brillouin zone, i.e., $q_v \to 0$, and the average phonon group velocities of each phonon branch were averaged in all Brillouin zone.

Fig. 1 (b) shows the schematic of the structrue and the thermal transfer in a graphene/hBN vdW heterostructure. Considering the vdW interface condition, the modified transmission coefficient of the j phonon mode with frequency ω_j for the vdW contact based on an improved acoustic mismatch model is

$$\tau_\omega^j = \frac{4z_1 z_2 \cos\theta_1 \cos\theta_2}{(z_1\cos\theta_2 + z_2\cos\theta_1)^2 + \frac{\omega_j^2}{K_A^2}(z_1 z_2 \cos\theta_1 \cos\theta_2)^2}. \quad (3)$$

The detailed derivation of Eq. (3) is shown in the electronic supplementary information (ESI) S1. The spring constant per unit area for graphene/hBN heterostructure is given by $K_A = nK$, where $n = 38.46$ nm^{-2} and $K_A = 9.72 \times 10^{19}$ kg·m^{-2}·s^{-2}. The acoustic impedance of the material/layer i ($i = 1$ or 2) in vdW heterostructures is $z_i = \rho_i v_{i,j}$, where ρ_i and $v_{i,j}$ are the mass density and the average group velocity of the phonon mode j, respectively. The angle between the interface normal and the phonon propagation direction in layers 1 and 2 is denoted by θ_i, which obeys Snell's law as $\sin\theta_1/v_1 = \sin\theta_2/v_2$ [see Fig. 1(b)]. In previous works, an incorrect transmission coefficient τ was derived and applied [9,13,23]. The initial contributors misplaced the acoustic impedances z_1 and z_2 by reversing their position at the denominator, leading to an error. Unfortunately, the follow-up works have failed to acknowledge and rectify this mistake, carrying forward the flawed expression. This work presents the correct Eq. (3) for transmission coefficient through vdW interactions. The updated formula is of significant importance and necessary for the relevant experimental studies.

Fig. 2 (b) and (c) show the phonon energy spectra and the acoustic phonon group velocities for graphene, hBN layers, and the corresponding heterostructure, calculated by DFT. The numerical average and maximum phonon group velocities $v_{i,j}$ are respectively shown in Table I. The transmission spectra of *ZA* acoustic phonons are displayed in Fig. 2(d). The *ZA* Phonons with frequencies below 1 THz can transmit through the vdW interface almost entirely, while the *ZA* phonons with frequencies above 10 THz are mostly unable to do so. This suggests that the low-frequency ZA phonons are most likely to penetrate through vdW-connected interfaces. Experimentally, the modulation of low-frequency ZA phonons can effectively control the thermal conductivity of the van der Waals interface. The results of our theoretical analysis are supported by the molecular dynamics simulations of Ref. [12]. Their simulation shows that the thermal conductivity in multilayer graphene/h-BN interface is dominantly contributed by the low-frequency phonons below 10 THz, and it decreases monotonically with increasing rotation angle between graphene and h-BN layer due to the enhanced interfacial phonon scattering. Our theoretical model can explain the results without rotations in their molecular dynamics simulations. The *ZA* phonon transmission spectrum blueshifts with increasing angle of incidence. We have observed the prominent differences between these results and those of the traditional welded interfaces ($K_A \to \infty$) [2].

Table 1 The calculated average and maximum *LA*, *TA*, and *ZA* phonon group velocities (km/s) of graphene, hBN, and their vdW heterostructure.

	Average			Maximum		
Velocity (km/s)	v_{LA}	v_{TA}	v_{ZA}	v_{LA}	v_{TA}	v_{ZA}
Graphene	8.94	6.54	3.74	21.89	13.81	8.22
hBN	9.49	7.97	2.56	19.65	12.12	6.28
Heterostructure	9.61	7.95	2.39	20.73	12.82	6.10

The gross thermal current per unit area J between the both layers including all the phonon mode j with the average velocity $v_{i,j}$ is given as

$$J = \frac{1}{2}\sum_j \int_0^{\omega_{jc_1}} \int_0^{\theta_{c_1}} N(\omega_j, T_1)\hbar\omega_j v_{1,j}\tau_\omega^j \cos\theta_1 \sin\theta_1 d\theta_1 d\omega_j - \frac{1}{2}\sum_j \int_0^{\omega_{jc_2}} \int_0^{\theta_{c_2}} N(\omega_j, T_2)\hbar\omega_j v_{2,j}\tau_\omega^j \cos\theta_2 \sin\theta_2 dd\theta_2 \omega_j, \quad (4)$$

with $N(\omega_j, T_i) = \omega_j^2/[2\pi^2 v_j^3(e^{\hbar\omega_j/k_B T_j} - 1)]$ being the density of phonon states at temperature T_i. The derivation process and additional modeling of Eq. (4) are shown in EIS S2. ω_{jc_i} and θ_{c_i} represent the cutoff frequency and the critical angle, respectively.

Fig. 2 (b) and (c) clearly demonstrate that graphene and hBN layers possess identical crystal structure, atomic mass density, and similar phononic properties [11]. As a result, the expression for gross thermal current per unit area J can be confidently established as

$$J = \frac{k_B^4 T_i^3 \Delta T}{\pi^2\hbar^3}\sum_j \int\int \frac{\tau_x^j x_j^3}{v_{i,j}^2(e^{x_j} - 1)} \cos\theta_i \sin\theta_i d\theta_i dx_j, \quad (5)$$

with $x_j = \hbar\omega_j/k_B T_i$. The termperature difference $\Delta T = |T_1 - T_2|$ is small, and

$$\tau_x^j = \frac{4z_1 z_2 \cos\theta_1 \cos\theta_2}{(z_1\cos\theta_2 + z_2\cos\theta_1)^2 + \eta x_j^2 (z_1 z_2 \cos\theta_1 \cos\theta_2)^2}, \quad (6)$$

with $\eta = k_B^2 T_i^2/(\hbar^2 K_A^2)$.

The interface thermal conductance per unit area is defined as

$$\kappa_I = \frac{J}{\Delta T} = \frac{k_B^2 K_A^2 T}{2\pi^2\hbar}\sum_j \int_0^{x_{j,c}} \frac{x_j \ln(1 + \beta_T^j x_j^2)}{z_j^2 v_j^2 (e^{x_j} - 1)} dx_j, \quad (7)$$

with $\beta_T^j = k_B^2 T^2 z_j^2/(4\hbar^2 K_A^2)$ and $x_{j,c} = \hbar\omega_{j,c}/k_B T$. $\omega_{j,c}$ is the cutoff frequency for the j phonon mode. The Kapitza thermal resistance can be computed as $R_I = 1/\kappa_I$. The values of $\omega_{LA,c}$, $\omega_{TA,c}$, and $\omega_{ZA,c}$ are estimated in Fig. 2(b) to be 24.1 THz, 18.0 THz, and 10.0 THz, respectively. These results are consistent with the reported findings [24]. In this work, the inter-plane acoustic transverse phonon mode ($j = TA$), the inter-plane acoustic longitudinal phonon mode ($j = LA$), and the ZA phonon mode ($j = ZA$) mentioned before are considered at low temperatures. $\rho = 2.28 \times 10^3$ kg/m^3 in graphene [25] and $\rho = 2.27 \times 10^3$ kg/m^3 in hBN layer [26]. It has been noticed that instead of using the maximum phonon group velocities listed in Table I, the average phonon group velocities should be used in vdW heterostructures

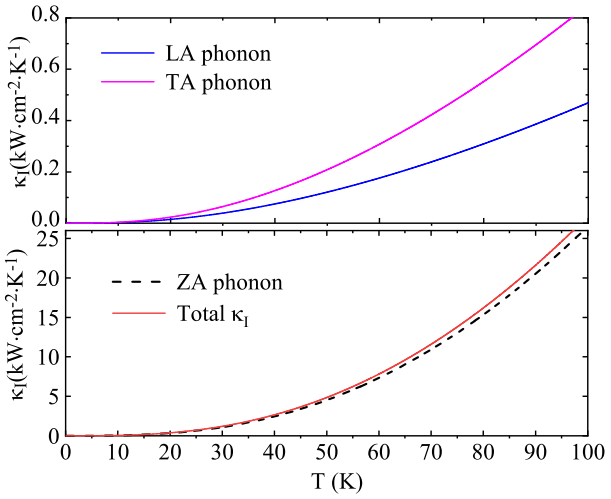

Fig. 3 The temperature dependence of the interfacial thermal conductance κ_I from *TA* and *LA* phonons (upper panel), *ZA* phonons, and the total interface thermal conductance (lower panel) in a graphene/hBN heterostructure.

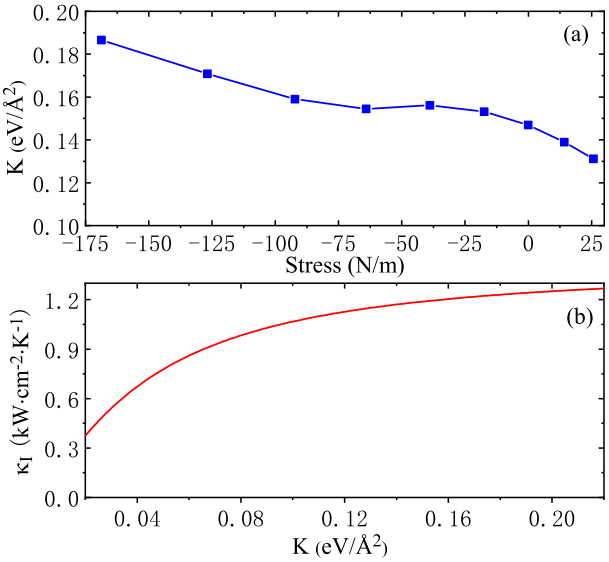

Fig. 4 (a) The vdW spring constant K as a function of stress and (b) the dependence of the total interface thermal conductance κ_I on K.

when calculating the heat conductances. Numerous research efforts to date have not distinguished between the two group velocities, which leads to an overestimation of the interface thermal conductivity[27,28].

Fig. 3 illustrates the temperature dependence of the interfacial thermal conductance κ_I induced by *TA* and *LA* phonons, *ZA* phonons, and the total interface thermal conductance. It reveals that the interfacial thermal conductivity κ_I is dominated by the *ZA* phonon modes, followed by the *TA* phonon, while the *LA* phonon has the smallest contribution. Previous studies have demonstrated comparable findings regarding bilayer graphene[26]. The contribution to conductivity increases with decreasing group velocity of acoustic phonons. Furthermore, the vdW interface connection determines that the impact of the *ZA* phonon is significant, while the *LA* phonon has minimal influence. At very low temperatures, the interfacial thermal conductivity is proportional to the third power of the temperature, namely $\kappa_I \sim T^3$ for $T \to 0$, which originates from the Debye's T^3 law of heat capacity; however, as the temperature increases, the interfacial thermal conductivity increases quasi-linearly with temperature, i.e. $\kappa_I \sim T$ for $T \gg 0$. The temperature dependence of the interface thermal conductivity results mainly from the vdW force connection. The energy of ZA phonons is lower than that of TA and LA phonons, and the frequency of ZA phonon modes is proportional to the square of the wavevector. The number of phonons increases more slowly with increasing temperature. Our results are in agreement with the experimental data[29,30]. The results differ significantly from both typical interface heat transport and those determined by molecular dynamics simulations.

Fig. 4 displays the vdW spring constant K as a function of stress (a) and the dependence of the total interface thermal conductance κ_I on K (b). The stress is applied biaxially, equally along a and b axes (in the xy plane). In VASP calculations, the pressure tensor represents the positive tensile stress applied[31]. When the lattice is compressed, the stress is negative, and vice versa. The structural optimization is achieved with every application of stress. From Fig. 4, we observe that the vdW spring constant K increases with increasing the strength of the stress. This implies that an increase in compressed stress results in a stronger vdW interaction between the layers. This is due to the fact that the increase of the compressive stress leads to a decrease in the equilibrium distance between the layers and an increase in vdW interaction energy. The detailed calculation data are included in ESI S3. The total interface thermal conductance κ_I shows a nonlinear dependence on the vdW spring constant K. As the spring constant increases, the thermal conductance increases. This behavior can be attributed to the stress-induced enhancement of vdW interactions. Recent experiments show that manipulating the coupling of the vdW interface can increase thermal boundary conductance[6]. Our study provides a detailed explanation of the experimental results supported by computational data.

All taken together, we have uncovered valuable insights into how heat transfer occurs through vdW interactions that are tuned by stress. In these considerations, the structure was optimized with every application of stress. The lattice mismatch is minimal in two-layer graphene/hBN heterostructures, and the interference from the substrate, impurities, or other factors was not considered, hence the impact of residual stress on the two monolayer materials was negligible. Nevertheless, we provide sufficiently convincing insights to argue that strain engineering can be used to design nanodevices that optimize thermal transport for the benefit of the desired performance.

3 Conclusion

In conclusion, a universal theoretical model is developed for interface thermal transport in both layers through vdW contacts, based on first-principles calculations at low temperatures. The heat transfer induced by vdW contacts is dominated by *ZA* phonons with low frequencies. The interface thermal conductivity increases non-linearly at low temperatures and quasi-linearly at el-

evated temperatures. The tuning of the interface thermal conductivity is effective through stress-controlled vdW interactions. Our theoretical model is widely applicable to vdW-bonded layers based on 2D materials. These insights suggest the technological value of utilizing stress points in developing novel vdW nanodevices with controlled thermal properties and advanced overall performance.

Author Contributions

Conceptualization: HMD, HPL, ZHT, MVM. Funding acquisition: HMD, YFD, MVM. Investigation: HMD, HPL, ZHT, YFD. Supervision: YFD, MVM, KC. Writing original draft: HMD, HPL. Writing review and editing: all authors.

Conflicts of interest

There are no conflicts to declare.

Acknowledgements

This work is supported by the Key Academic Discipline Project of China University of Mining and Technology (No. 2022WLXK03), the National Natural Science Foundation of China (Grant No. 12374079), and the Research Foundation-Flanders (FWO).

Notes and references

1 S. E. Kim, F. Mujid, A. Rai *et al.*, *Nature*, 2021, **597**, 660–665.
2 J. Chen, X. Xu, J. Zhou *et al.*, *Reviews of Modern Physics*, 2022, **94**, 025002.
3 H. M. Dong, P. P. Fu, Y. F. Duan and K. Chang, *Nanoscale*, 2023, **15**, 15643–15648.
4 N. Bonini, J. Garg and N. Marzari, *Nano Letters*, 2012, **12**, 2673–2678.
5 K. Y. Fong, H.-K. Li, R. Zhao *et al.*, *Nature*, 2019, **576**, 243–247.
6 B. Xu, S. Hu, S.-W. Hung *et al.*, *Science Advances*, 2021, **7**, eabf8197.
7 W. Yuan, K. Ueji, T. Yagi *et al.*, *ACS Nano*, 2021, **15**, 15902–15909.
8 Z.-Y. Ong, G. Zhang and Y.-W. Zhang, *Physical Review B*, 2016, **93**, 075406.
9 R. Prasher, *Applied Physics Letters*, 2009, **94**, 041905.
10 X. Gu, Y. Wei, X. Yin *et al.*, *Reviews of Modern Physics*, 2018, **90**, 041002.
11 D. Wang, G. Chen, C. Li *et al.*, *Physical Review Letters*, 2016, **116**, 126101.
12 W. Ren, Y. Ouyang, P. Jiang *et al.*, *Nano Letters*, 2021, **21**, 2634–2641.
13 J. Yang, Y. Yang, S. W. Waltermire *et al.*, *Nature Nanotechnology*, 2012, **7**, 91–95.
14 G. Kresse and J. Hafner, *Phys. Rev. B*, 1994, **49**, 14251–14269.
15 G. Kresse and J. Furthmüller, *Phys. Rev. B*, 1996, **54**, 11169–11186.
16 P. E. Blöchl, *Phys. Rev. B*, 1994, **50**, 17953–17979.
17 G. Kresse and D. Joubert, *Phys. Rev. B*, 1999, **59**, 1758–1775.
18 J. P. Perdew, K. Burke and M. Ernzerhof, *Phys. Rev. Lett.*, 1996, **77**, 3865–3868.
19 S. Grimme, S. Ehrlich and L. Goerigk, *Journal of Computational Chemistry*, 2011, **32**, 1456–1465.
20 L. Goerigk and S. Grimme, *Phys. Chem. Chem. Phys.*, 2011, **13**, 6670–6688.
21 L. Lindsay and D. A. Broido, *Physical Review B*, 2012, **85**, 035436.
22 A. Togo and I. Tanaka, *Scripta Materialia*, 2015, **108**, 1–5.
23 W. A. Little, *Canadian Journal of Physics*, 1959, **37**, 334.
24 S. Ghosh, D. L. Nika, E. P. Pokatilov and A. A. Balandin, *New Journal of Physics*, 2009, **11**, 095012.
25 X. Cong, Q.-Q. Li, X. Zhang *et al.*, *Carbon*, 2019, **149**, 19–24.
26 A. I. Cocemasov, D. L. Nika and A. A. Balandin, *Nanoscale*, 2015, **7**, 12851–12859.
27 D. L. Nika and A. A. Balandin, *Reports on Progress in Physics*, 2017, **80**, 036502.
28 I. Jo, M. T. Pettes, J. Kim *et al.*, *Nano Letters*, 2013, **13**, 550–554.
29 C.-C. Chen, Z. Li, L. Shi and S. B. Cronin, *Applied Physics Letters*, 2014, **104**, 081908.
30 K. F. Mak, C. H. Lui and T. F. Heinz, *Applied Physics Letters*, 2010, **97**, 221904.
31 X. Peng, Q. Wei and A. Copple, *Phys. Rev. B*, 2014, **90**, 085402.